Feedback noncausal model predictive control of wave energy converters

Siyuan Zhan[a], Guang Li[a,*], Jing Na[b], Wei He[c]

[a]School of Engineering and Material Science, Queen Mary University of London, 327 Mile End Rd., London, E1 4NS, UK
[b]Faculty of Mechanical and Electrical Engineering, Kunming University of Science and Technology, South Jingming Rd., Kunming, 650500, China
[c]School of Automation and Electrical Engineering, University of Science and Technology Beijing, Xueyuan Rd, Beijing, 100083, China

Abstract

In this paper, a novel feedback noncausal model predictive control (MPC) strategy for sea wave energy converters (WECs) is proposed, where the wave prediction information can be explicitly incorporated into the MPC strategy to improve the WEC control performance. The main novelties of the MPC strategy proposed in this paper include: (i) the recursive feasibility and robust constraints satisfaction are guaranteed without a significant increase in the computational burden; (ii) the information of short-term wave prediction is incorporated into the feedback noncausal MPC method to maximise the potential energy output; (iii) the sea condition for the WEC to safely operate in can be explicitly calculated. The proposed feedback noncausal MPC algorithm can also be extended to a wide class of control design problems, especially to the energy maximisation problems with constraints to be satisfied and subject to persistent but predictable disturbances. Numerical simulations are provided to show the efficacy of the proposed feedback noncausal MPC.

Keywords: Wave energy converters, feedback model predictive control, recursive feasibility, wave predictions.

1. Introduction

Ocean waves provide considerable sustainable energy sources (Salter, 1974). It is estimated that there are 25 trillion watts (TWs) of power in ocean waves worldwide and within the UK the power potential is roughly 7-10 gigawatts (GWs) (Thorpe et al., 1999). Two of the main advantages of using wave energy over more mature renewable energy sources, such as wind energy and solar energy, are its high power density and persistence (Falnes, 2007). The technology of harnessing energy from sea waves has received extensive research attention, especially after the oil crisis in 1970s. Many types of wave energy converters (WECs) have been invented to extract wave energy, e.g. point absorbers (Budar and Falnes, 1975) and attenuators (Henderson, 2006). Despite the great potential of wave energy, its cost per kilowatt hour (kWh) is still relatively high compared with solar energy and wind energy.

To reduce the unit cost of wave energy, various types of control strategies have been proposed to increase the energy conversion rate (Drew et al., 2009). Based on the impedance matching principle, that is, the maximal wave energy power output can be achieved when the natural frequency of a WEC matches the dominant frequency of the incoming waves (Falnes, 2002), some feedforward control algorithms have been adopted, e.g. latching control (Babarit and Clément, 2006), phase control (António, 2008) and declutching control (Babarit et al., 2009). Whilst this type of control algorithms are effective under regular waves, they can become complicated to implement in real irregular sea wave conditions (Salter et al., 2002).

In recent years, to improve performance of WECs in complex real sea conditions, some novel optimisation-based control algorithms have been developed, e.g. optimal control (Zhan and Li, 2018), pseudo-spectral control (Li, 2017; Mérigaud and Ringwood, 2018) and moment matching control (Faedo et al., 2018). It is shown (Fusco and Ringwood, 2013; Cretel et al., 2011; Brekken, 2011; Hals et al., 2011) that the WEC control problem is essentially a constrained optimal control problem subject to persistent disturbances, and it has been widely acknowledged that the model predictive control (MPC) can be very effective in optimising control objectives while handling both state and control input constraints (Mayne et al., 2000). With the development of wave prediction technology, e.g. short-term wave forecasting (STWF) (Fusco and Ringwood, 2010; Mérigaud and Ringwood, 2018) and deterministic sea wave prediction (DSWP) (Belmont et al., 2014), it has been demonstrated (Li et al., 2012; Li and Belmont, 2014) that the efficiency of WECs can be significantly improved by incorporating wave predictions into MPC design. Although the existing WEC MPC algorithms can explicit handle both input and state constraints, not much attention has been given to the feasibility issue, that is, the online optimisation of MPC cannot give a feasible solution and sometimes can even lead to a catastrophic failure (Bemporad and Morari, 1999). The proposed noncausal feedback MPC can be applied to different types of WECs; however, for demonstration purpose, we use a benchmark point absorber to demonstrate its efficacy.

In fact, to guarantee the robust feasibility and robust constraint satisfaction, MPC has to be implemented where the control actions are derived from feedback policies (Mayne et al., 2000; Goulart et al., 2006). Due to this fact, a feedback causal

*Address all correspondence to this author.
Email address: g.li@qmul.ac.uk (Guang Li)

MPC algorithm for the WEC control problem is proposed in our recent work (Zhan et al.) that explicitly addressed the issues of recursive feasibility and robust constraint satisfaction. However, without using the future wave information, the resulting feedback causal MPC of WEC can only yield a sub-optimal control policy.

Motivated by the fact that the WEC control problem is essentially a non-causal optimal control problem and the the future wave prediction can play a nontrivial role in improving WEC control performance, we propose a novel feedback noncausal MPC algorithm for WEC that tackles the non-causality problem, which was not resolved in (Zhan et al.). This noncausal MPC allows incorporation of the short-term future wave prediction to improve the energy conversion efficacy of a WEC. The novelty of this algorithm is that the information of future wave information can be explicitly incorporated in to current control action, which results in a significant performance improvement over the feedback causal MPC proposed in (Zhan et al.). The features of recursive feasibility and robust constraints satisfaction are shown to be preserved via a special tailored constraint tighten approach (Chisci et al., 2001). Extensive simulation results are presented to demonstrate the effectiveness and robustness of the proposed MPC, and also the superior energy output performance over the other causal optimal control methods.

The remaining of the paper is organised as follows. The WEC dynamics are described in Section 2. Sections 3 and 4 show the formulation and implementation of the robust noncausal WEC MPC, respectively. Numerical simulations are provided in Section 5 and the paper is concluded in Section 6.

Notations: Let $\mathbb{R}^n$ denote the space of real n-dimensional vectors; $\mathbb{I}_{\geq a}$ denotes the integers greater than or equal to a; $\mathbb{I}_{[a,b]}$ denotes the integers from a to b. For column vectors $\mathbf{a}$ and $\mathbf{b}$, $[\mathbf{a}, \mathbf{b}]$ denotes the column vector $[\mathbf{a}^T\ \mathbf{b}^T]^T$; $\boldsymbol{v}_{[a,b]}$ denotes column vector $[v(i), v(i+1), \ldots, v(j)]$; $\rho(A)$ denotes the spectral radius of a matrix A; n_p and n_x are the wave prediction length and the number of states respectively.

For the subsets $\mathbb{A} \subset \mathbb{R}^n$ and $\mathbb{B} \subset \mathbb{R}^n$, the Minkowski set addition is defined by $\mathbb{A} + \mathbb{B} \triangleq \{a + b : a \in \mathbb{A}, b \in \mathbb{B}\}$. The P-subtraction is defined by $\mathbb{A} \sim \mathbb{B} \triangleq \{a \in \mathbb{R}^n : a + b \in \mathbb{A}, \forall b \in \mathbb{B}\}$. For $\mathbb{A} \subset \mathbb{R}^n$ and matrix M with compatible dimensions, $M\mathbb{A} \triangleq \{Ma : a \in \mathbb{A}\}$.

2. WEC dynamic modelling

In this paper, a particular type of WEC called point absorber is studied to show the efficacy of our proposed method. However, the feedback noncausal MPC strategy proposed in this paper is generic and can be extended to other types of WECs.

Fig. 1 illustrates the working principle of a point absorber. z_w is the wave level; the buoy is floating on the sea surface, whose heave displacement is z_v; below the buoy is a hydraulic cylinder fixed to the seabed. The persistent wave excitation force drives the buoy, which provides relative motion between the piston fixed to the buoy and the cylinder fixed to the seabed. The kinetic energy of the relative motion can be captured by a power

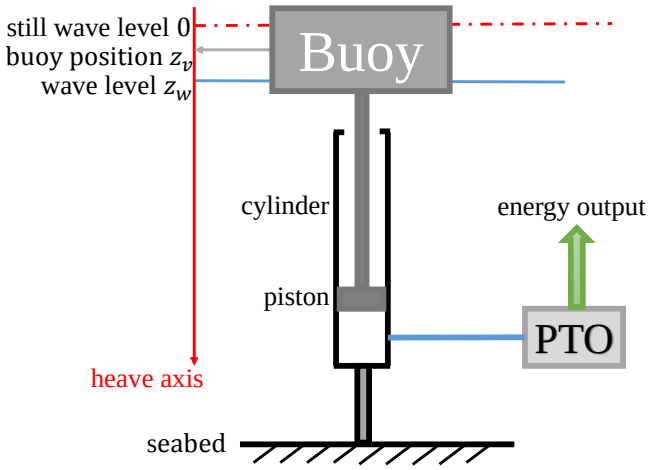

Figure 1: Schematic diagram of the working principle of a point absorber

take-off (PTO) mechanism to generate electricity. The PTO mechanisms vary from device to device, and can be realised by a hydraulic motor attached to a high-speed rotary electrical generator (Mueller, 2002; Kim et al., 2001) or by a direct electrical linear generator (Baker and Mueller, 2001; Drew et al., 2009). Since in both cases the generator force or torque is proportional to the force f_u exerted on the piston, the force f_u can be used directly as the control input without lost of generality. Note that the mooring force needs also considered in the WEC dynamic modelling especially for floating WECs (Richter et al., 2013a,b; Amann et al., 2015); however, the mooring force is not involved in this case study since the cylinder is assumed to be directly fixed to the seabed. The proposed noncausal MPC strategy can also be extended to two-body floating WEC subject to mooring force.

The piston moves together with the buoy at a heave velocity $\dot{z}_v$. The potential power that can be captured by the PTO at time t is

$$P(t) = -f_u(t)v(t) \tag{1}$$

and the energy absorbed in a time interval $[T_1, T_2]$ can be expressed by

$$E = \int_{T_1}^{T_2} -f_u(t)v(t)dt \tag{2}$$

For safe operation purpose, a set of constraints are imposed on the WEC heave displacement and heave velocity, which can be expressed by

$$\begin{aligned} |z_v| &\leq d_{\max} \\ |\dot{z}_v| &\leq v_{\max} \end{aligned} \tag{3}$$

where $z_{\max}$ and $v_{\max}$ are the maximal allowed heave displacement and heave velocity respectively.

The other aspect to be considered is the capacity of PTO system, which can be represented by a limitation of control input force

$$|f_u| \leq u_{\max} \tag{4}$$

Here, $u_{\max}$ is the maximal value of the control input force that can be produced by the PTO mechanism. For a given sea condition over a period, the wave magnitude is assumed to be bounded by $w_{\max}$ as

$$|z_w| \leq w_{\max} \tag{5}$$

At each time, a t_p length prediction of the future wave amplitude $\tilde{\boldsymbol{w}}$ is provided by the short-time wave prediction techniques, e.g. (Mérigaud and Ringwood, 2018; Belmont et al., 2014) based on the measured current wave elevation $\tilde{w}$. Consequently, the WEC control to be developed is indeed noncausal since the future wave prediction is integrated into the control implementation. The use of future wave prediction can contribute to increasing the energy output in comparison to the causal controllers, which has been well-recognised in the WEC control field, and will be validated in simulations in this paper.

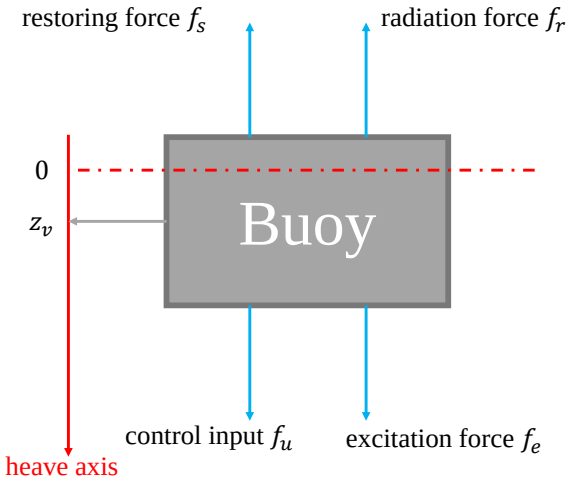

Figure 2: Dynamic diagram of the point absorber

The WEC controller design objective is to maximise the energy output (2) for a period of time subject to constraints (3) and (4) under the sea condition (5).

The WEC dynamic modelling procedure follows the work of (Yu and Falnes, 1995) and is briefly described here for completeness. The dynamic modelling of the point absorber is illustrated in Fig. 2. By applying Newton's second law, the dynamics of WEC can be modelled by

$$m_s \ddot{z}_v = f_e - f_s - f_r + f_u \tag{6}$$

where m_s is the mass of the buoy with the attached piston; f_s is the restoring force that can be computed by

$$f_s = k_s z_v \tag{7}$$

with the hydro-stiffness coefficient given by $k_s = \rho g S$. Here ρ is the water density; g is the acceleration of gravity; S is the cross sectional area of the floating buoy. f_u is the force provided by PTO and is treated as the control input. f_r and f_e are the frequency dependent radiation force and excitation force, respectively.

The radiation force is determined by

$$f_r = m_\infty \ddot{z}_v + f_R \tag{8a}$$

where m_∞ is called frequency-independent added mass; f_R is the noncausal convolutional part of the radiation force and can be computed by

$$f_R = \int_{-\infty}^{\infty} h_r(\tau)\dot{z}_v(t-\tau)d\tau \tag{8b}$$

where the kernel of the radiation force h_r can be numerically calculated via hydro-dynamic software packages (e.g. NEMO (Lima et al., 2011), WAMIT (Lee, 1995)), which can be approximated by a causal state-space representation (Yu and Falnes, 1995)

$$\begin{aligned} \dot{x}_r &= A_r x_r + B_r \dot{z}_v \\ f_R &\approx C_r x_r \end{aligned} \tag{8c}$$

where $D_r(s) \sim (A_r, B_r, C_r, 0)$ and x_r are the state-space realisation and the associated state respectively. Following the similar route as the above derivation, the persistent wave excitation force can be modelled by

$$f_e = \int_{-\infty}^{\infty} h_e(t - t_c - \tau) z_w(\tau) d\tau \tag{9a}$$

with h_e being the excitation kernel, which can be approximated by the following state-space formulation

$$\begin{aligned} \dot{x}_e &= A_e x_e + B_e z_w \\ f_e &= C_e \tilde{x}_e \end{aligned} \tag{9b}$$

where $\tilde{x}_e = x_e(t + t_c)$ with t_c as a positive constant non-causal time shift, $D_e(s) \sim (A_e, B_e, C_e, 0)$ and x_e are the state-space realisation and the associated state respectively.

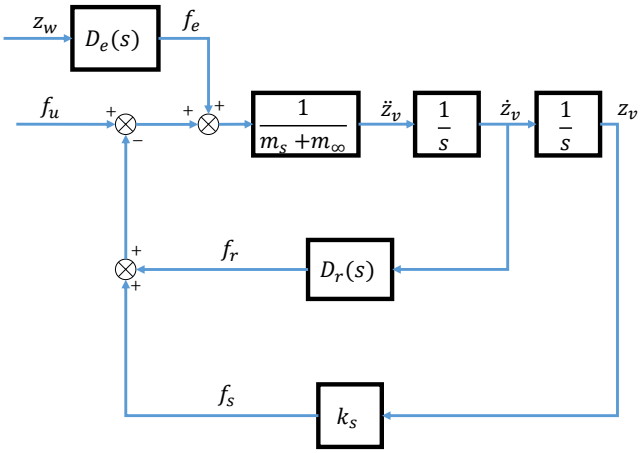

Figure 3: Block diagram of the point absorber

The block diagram of the WEC dynamics model is shown in Fig. 3. With relisations of (8) and (9), the state-space model of the WEC can be established by

$$\begin{cases} \dot{x} = A_c x + B_{uc} u + B_{wc} w \\ z = C_z x \end{cases} \tag{10}$$

where $w := z_w$, $z := z_v$, $y := \dot{z}_v$, $x := [z_v, \dot{z}_v, x_r, \tilde{x}_e]$ and

$$A_c = \begin{bmatrix} 0 & 1 & 0 & 0 \\ -\frac{k_s}{m} & 0 & \frac{C_e}{m} & -\frac{C_f}{m} \\ 0 & B_r & A_r & 0 \\ 0 & 0 & 0 & A_e \end{bmatrix} \; B_{wc} = \begin{bmatrix} 0 \\ 0 \\ 0 \\ B_e \end{bmatrix} \; B_{uc} = \begin{bmatrix} 0 \\ \frac{1}{m} \\ 0 \\ 0 \end{bmatrix} \tag{11}$$
$$C_z = \begin{bmatrix} 0 & 1 & 0_{1\times(n_r+n_e)} \end{bmatrix}$$

with $m := m_s + m_\infty$. Here, n_r and n_e are the number of states associated with radiation force (8) and excitation force (9) respectively. Note that when the convolution terms in the radiation force (8) and excitation force (9) are approximated by $f_R = D_r \dot{z}_v$ and $f_e = D_e z_w$ respectively, then the state-space model of (11) can be reduced to a 2^{nd}-order model as studied in (Li and Belmont, 2014).

To develop the robust noncausal MPC, the model (10) is converted to a discrete-time model with sampling time t_s, as given by

$$\begin{cases} x(k+1) = Ax(k) + B_u u(k) + B_w w(k) \\ z(k) = C_z x(k) \end{cases} \tag{12}$$

and the wave prediction length is represented by n_p steps satisfying $t_p = n_p t_s$.

3. Feedback noncausal MPC formulation

3.1. Construction of noncausal MPC

To formulate the feedback noncausal MPC design, the state and input constraints (3)-(4) are represented by $x \in \mathbb{X}$ and $u \in \mathbb{U}$ respectively, where $\mathbb{X}$ and $\mathbb{U}$ are defined by

$$\begin{aligned} \mathbb{X} &:= \{x \in \mathbb{R}^{n_x} : |x_1| \le z_{\max} \;\&\; |x_2| \le v_{\max}\} \\ \mathbb{U} &:= \{u \in \mathbb{R} : |u| \le u_{\max}\} \end{aligned} \tag{13}$$

and from (5), the wave disturbance is bounded by $w \in \mathbb{W}$, where $\mathbb{W}$ is defined by

$$\mathbb{W} := \{w \in \mathbb{R} : |w| \le w_{\max}\} \tag{14}$$

Assumption 1. *The pairs (A, B_u) and (A, C_s) from the discrete-time system* (12) *is controllable and observable, where $C_s := \begin{bmatrix} 1_{2\times 2} & 0_{2\times(n_r+n_e)} \end{bmatrix}$.*

Note that this assumption holds for most WEC control problems. The WEC MPC can be redefined as: to design control strategies at each sampling time, and find a control sequence $\boldsymbol{u}$ using the information of current state x and a n_p-step of future wave prediction $\tilde{\boldsymbol{w}} := [\tilde{w}(k), \tilde{w}(k+1), \ldots, \tilde{w}(k+n_p-1)]$ by recursively solving the following constrained optimisation problem

$$\min_{\boldsymbol{u}} \lim_{N\to\infty} \frac{1}{N} \sum_{k=0}^{N-1} \ell(x(k), u(k)) \tag{15a}$$
$$\text{s.t. } x(k+1) = Ax(k) + B_u u(k) + B_w w(k) \tag{15b}$$
$$x(k) \in \mathbb{X},\; u(k) \in \mathbb{U},\; \forall w(k) \in \mathbb{W},\; \forall k \in \mathbb{I}_{\ge 0} \tag{15c}$$

where the stage cost $\ell(x(k), u(k))$ is given by

$$\ell(x(k), u(k)) := \frac{1}{2} x(k)^T Q x(k) + \frac{1}{2} r u(k)^2 + z(k) u(k) \tag{16}$$

Here in the stage cost (16), the first two terms $\frac{1}{2}x(k)^T Q x(k) + \frac{1}{2} r u(k)^2$ are used to penalise the state and control input respectively; the weights Q and r can be used as tuning parameters to influence the stability and robustness of the system; $-z_k u_k$ represents the power at time step k that can be absorbed by the PTO mechanism.

Before proceeding to the formulation of feedback noncausal MPC, we first start with the unconstrained case, i.e. the constraints on input and state (15c) are assumed to be inactive. The result in (Zhan and Li, 2018) shows that when constraints are inactive and with a proper tuning of coefficients Q and r and sufficiently long wave prediction horizon n_p, the optimisation problem described in (15) can be resolved by a linear noncausal control strategy, as described in the following lemma:

Lemma 1. *[Linear noncausal optimal control (Zhan and Li, 2018)] When constraints* (15c) *are inactive, the infinite dimensional optimisation problem defined in* (15) *can be tackled by the following linear noncausal optimal control policy without performance degradation*

$$u = K_x x + K_d \tilde{\boldsymbol{w}} \tag{17a}$$

where $\tilde{\boldsymbol{w}}$ is the n_p-step of wave prediction; x is the current state; the coefficients K_x and K_d are determined from

$$K_x = -(r + B_u^T V B_u)^{-1}(C_z + B_u^T V A) \tag{17b}$$
$$K_d = -(r + B_u^T V B_u)^{-1} B_u^T \Psi \tag{17c}$$

where V is the solution of the discrete-time algebraic Ricatti equation (DARE)

$$\begin{aligned} V = {} & A^T V A + Q \\ & - (B_u^T V A + C_z)^T (r + B_u^T V B_u)^{-1} (B_u^T V A + C_z) \end{aligned} \tag{17d}$$

and $\Phi = (A + B_u K_x)^T$; $\Psi := [V B_w, \Phi V B_w, \ldots, \Phi^{n_p-1} V B_w]$, provided that the DARE (17d) *yields a unique stabilising solution and the wave prediction length n_p is long enough.*

Remark 1. *With a proper tuning of Q and r, $A_K := A + BK_x$ is exponentially stable, i.e. $\rho(A_K) < 1$. More details of choosing the weights Q and r and the wave prediction length n_p for the above noncausal optimal control can be found in (Zhan and Li, 2018).*

Although the linear noncausal optimal control policy described in Lemma 1 provides a fast and easy WEC control design method, the linear noncausal optimal control only works when constraints are inactive, which limits its applications, especially when the constraints violations become a critical issue in large wave conditions.

In the following, based on the linear noncausal optimal control policy, we propose a robust non-causal MPC that can explicitly handle the constraints. Many existing robust feedback

MPC algorithms (Lee and Kouvaritakis, 2000; Chisci et al., 2001) adopt the control policies that include a state feedback term to optimise the performance and an online optimisation variable to cope with hard constraints. Inspired by these results, this paper proposes a feedback noncausal MPC policy

$$u(x, \tilde{\boldsymbol{w}}) = K_x x + K_d \tilde{\boldsymbol{w}} + v \tag{18}$$

where the first two terms are the pre-designed linear noncausal optimal controller computed via Lemma 1 to maximise the energy output for the unconstrained system and guarantee the nominal stability of the system; the last term v is the optimisation variable determined online to cope with state and input constraints. The working principle of the proposed robust noncausal MPC can be summarised as follows:

1. When constraints are inactive, $v = 0$ and the robust noncausal feedback MPC degenerates to a linear noncausal optimal control.
2. When constraints are active, $v \neq 0$ and it is used to keep the constraints satisfied.

The design concept of the robust noncausal MPC (18) is to minimise the effect of v in the control performance so that an optimal performance can be achieved when the trajectory of the robust noncausal MPC is close to the well tuned linear noncausal optimal control as described in Lemma 1.

Algorithm 1. *The feedback noncausal MPC problem can be implemented at each time step k by recursively solving the following optimisation problem with the state information x and a n_p-step wave prediction $\tilde{\boldsymbol{w}}$*

$$\boldsymbol{v}^*_{[0,\infty]} = \arg\min_{\boldsymbol{v}_{[0,\infty]}} \sum_{k=0}^{\infty} v^2(k) \tag{19a}$$

$$s.t.\ \ x(k+1) = Ax(k) + B_u u(k) + B_w w(k) \tag{19b}$$

$$u(k) = K_x x(k) + K_d E^k \tilde{\boldsymbol{w}} + v(k) \tag{19c}$$

$$x(0) = x \tag{19d}$$

$$x(k) \in \mathbb{X},\ u(k) \in \mathbb{U},\ \forall w(k) \in \mathbb{W},\ \forall k \in \mathbb{I}_{\geq 0} \tag{19e}$$

where $\boldsymbol{v}_{[0,\infty]} := [v(0), v(1), \dots]$; K_x and K_d are the offline designed linear noncausal optimal control coefficients determined from Lemma 1; E is the translation matrix

$$E := \begin{bmatrix} 0_{(n_p-1)\times 1} & I_{n_p-1} \\ 0 & 0_{1\times(n_p-1)} \end{bmatrix}$$

and apply

$$u = K_x x + K_w \tilde{\boldsymbol{w}} + v_0^*$$

to the system, where v_0^* denotes the first element of $\boldsymbol{v}^*_{[0,\infty]}$.

Note that for safe operation purpose, in Algorithm 1 the state and control input constraints (19e) are required to be satisfied for all realisation of $w \in \mathbb{W}$ and for all time $k \in \mathbb{I}_{\geq 0}$. However, Algorithm 1 is not practically implementable because of the universal quantifier in (19) and the infinite dimension of the optimisation problem.

3.2. Constraints handling of robust noncausal MPC

In this section, a specifically tailored constraint tightening approach is adopted to make Algorithm 1 implementable. To eliminate the infinite dimension problem, after n_p steps, the constraints are assumed to be inactive, i.e. $v(k) = 0$ for $k \in \mathbb{I}_{\geq n_p}$ and the resulting linear state feedback terminal local controller $u(k) = K_x x(k)$ can be derived from (19c). The feedback noncausal MPC control can be summarised by

$$u(k) = \begin{cases} K_x x(k) + K_d E^k \tilde{\boldsymbol{w}} + v(k), & k \in \mathbb{I}_{[0,n_p-1]} \\ K_x x(k), & k \in \mathbb{I}_{\geq n_p} \end{cases} \tag{20}$$

The system (12) with a feedback noncausal policy (20) can be represented by

$$x(k+1) = \begin{cases} A_K x(k) + B_u K_d E^k \tilde{\boldsymbol{w}} + B_u v(k) + B_w w(k), & k \in \mathbb{I}_{[0,n_p-1]} \\ A_K x(k) + B_w w(k), & k \in \mathbb{I}_{\geq n_p} \end{cases} \tag{21}$$

where $A_K := A + B_u K_x = \Phi^T$. Next, it will be shown that the satisfaction of constraints on state $x(k) \in \mathbb{X}$ and control input $u(k) \in \mathbb{U}$ for all realisations of $w(k) \in \mathbb{W}$ with terminal local controller $u(k) = K_x x(k)$ can be guaranteed by imposing a terminal controller on the state $x(n_p)$. This formulation relies on the concept of the maximal output admissible set (MOAS) as defined below:

Definition 1 (MOAS (Kolmanovsky and Gilbert, 1995))**.** *The MOAS Σ of system* (12) *with a terminal local controller $u = K_x x$ subject to state and input constraints $x \in \mathbb{X}$ and $u \in \mathbb{U}$ and the persistent disturbance $w \in \mathbb{W}$ is defined by*

$$\Sigma := \left\{ x(0) \in \mathbb{X} : \begin{array}{l} x(k+1) = A_K x(k) + B_w w(k) \\ x(k) \in \mathbb{X},\ K_x x(k) \in \mathbb{U} \\ \forall w(k) \in \mathbb{W},\ \forall k \in \mathbb{I}_{\geq 0} \end{array} \right\} \tag{22}$$

Remark 2. *Since the state and control input constraints defined by* (13) *and* (14) *are polytopes and $\rho(A_K) < 1$, the MOAS Σ is a polytope and can be finitely determined (Kolmanovsky and Gilbert, 1995).*

Next, following the similar procedures of (Zhan et al.; Chisci et al., 2001), the universal quantifier problem is resolved by introducing a pair of auxiliary prediction system and tightened constraints.

Definition 2 (Auxiliary prediction system)**.** *The auxiliary prediction system for $k \in \mathbb{I}_{[0,n_p-1]}$ is defined by*

$$\begin{aligned} \bar{x}(k+1) &= A\bar{x}(k) + B_u \bar{u}(k) \\ \bar{u}(k) &= K_x \bar{x}(k) + K_d E^k \tilde{\boldsymbol{w}} + + v(k) \\ \bar{x}(0) &= x(0) = x \end{aligned} \tag{23}$$

Definition 3 (Tightened constraints)**.** *The tightened constraints for the auxiliary system* (23) *are defined by $\bar{x}(k) \in \mathbb{X}_k$, $\bar{u}(k) \in \mathbb{U}_k$ for $k \in \mathbb{I}_{[0,n_p-1]}$ and $\bar{x}(n_p) \in \mathbb{X}_T$, where*

$$\begin{array}{ll} \mathbb{X}_k := \mathbb{X} \sim \mathbb{E}_k, & \mathbb{U}_k := \mathbb{U} \sim K_x \mathbb{E}_k, \\ \mathbb{E}_k := \sum_{i=0}^{k-1} A_K^i B_w \mathbb{W}, & \mathbb{X}_T := \Sigma \sim \mathbb{E}_{n_p}. \end{array} \tag{24}$$

Lemma 2. *The requirement of constraints satisfaction of all time and all realisations of disturbance w can be guaranteed via imposing the tightened constraints* (24) *on the auxiliary prediction system* (23)*.*

Proof. The proof is similar to (Chisci et al., 2001), and can be shown by comparing the state and control trajectories of system (21) with the feedback noncausal MPC control policy (20) with those of the auxiliary prediction system (23) such that

$$\begin{aligned} x(k) &= \bar{x}(k) + \sum_{i=1}^{k} A_K^{i-1} B_w w(k-i) \\ u(k) &= \bar{u}(k) + \sum_{i=1}^{k} A_K^{i-1} B_w w(k-i) \end{aligned} \tag{25}$$

The tightened constraints in (24) are satisfied for the trajectories of the auxiliary prediction system (23), which implies $x(k) \in \mathbb{X}$, $u(k) \in \mathbb{U}$ for $k \in \mathbb{I}_{[0,n_p-1]}$ and $x(t+n_p) \in \Sigma$. Then the proof is completed with Definition 1. □

Remark 3. *With Lemma 2, the intractable optimisation problem* (19) *can be converted to the following optimisation problem*

$$\begin{aligned} \boldsymbol{v}^*_{[0,n_p-1]} = \ & \arg\min_{\boldsymbol{v}_{[0,n_p-1]}} \sum_{k=0}^{n_p-1} v^2(k) \\ s.t. \ & \bar{x}(k+1) = A\bar{x}(k) + B_u\bar{u}(k) \\ & \bar{u}(k) = K_x\bar{x}(k) + K_d E^k \tilde{\boldsymbol{w}} + v(k) \\ & \bar{x}(0) = x \\ & \bar{x}(k) \in \mathbb{X}_k, \ \bar{u}(k) \in \mathbb{U}_k, \ \forall k \in \mathbb{I}_{[0,n_p-1]} \\ & \bar{x}(n_p) \in \mathbb{X}_T \end{aligned} \tag{26}$$

where the set $\mathbb{X}_k$, $\mathbb{U}_k$ and $\mathbb{X}_T$ are defined in (24)*.*

Lemma 3 (Recursive feasibility)**.** *The online recursively solved optimisation problem* (26) *is always feasible provided that the initial state is feasible.*

Proof. The proof can be easily shown by defining $b(k) = v(k) + K_d E^k \boldsymbol{w}$, and applying Lemma 7 from (Chisci et al., 2001). □

Remark 4. *The recursive feasibility of such a feedback MPC with explicit incorporation of wave prediction can be guaranteed by the existence of the MOAS described in Definition 1. The tuning of weights Q and r not only affects the energy output, but also determines the sea conditions under which the MOAS* (22) *exists. In fact, when tuning these weights, there is a trade-off between the energy conversion efficiency and the robustness so that the WEC can safely work in the worst sea wave scenario in a sea state. Generally speaking, the WEC feedback MPC controller needs to be tuned using small weights on Q and r to have a better energy conversion efficiency in a mild sea state, while in a high sea state the WEC feedback MPC controller needs to be tuned using large weights Q and r to obtain a better robustness so that the state and input constraints can be satisfied. In addition, with Assumption 1, all the states are guaranteed to be bounded. This can be also refereed as the Uniformly Ultimate Boundedness (UUB) of the system states.*

To make the feedback noncausal MPC algorithm directly implementable, it will be shown in Section 4 that the online recursively resolved optimisation problem (26) can be formulated and implemented via a quadratic programming (QP) algorithm.

4. Implementations

4.1. QP formulation of the feedback noncausal MPC

In this subsection, the optimisation problem (26) is converted to a QP problem. The objective function can be rewritten as

$$J \triangleq \boldsymbol{v}^T_{[0,n_p-1]} \boldsymbol{v}_{[0,n_p-1]} \tag{27}$$

The predicted state trajectory from the auxiliary prediction system (23) is

$$\bar{x}(k) = A_K^k x + \boldsymbol{M}_k \boldsymbol{v}_{[0,n_p-1]} + \boldsymbol{C}_k \tilde{\boldsymbol{w}} \tag{28a}$$

for $k \in \mathbb{I}_{[0,n_p]}$, where $\boldsymbol{M}_k \in \mathbb{R}^{n_x \times n_p}$ is given by

$$\boldsymbol{M}_k := \begin{bmatrix} A_K^{i-1}B_u & A_K^{i-2}B_u & \dots & B_u & 0 & \dots & 0 \end{bmatrix}$$

and $\boldsymbol{C}_k \in \mathbb{R}^{n_x \times n_p}$ is given by

$$\boldsymbol{C}_k := \begin{cases} 0_{n_x \times n_p}, & k = 0 \\ \begin{bmatrix} 0 & \dots & 0 & B_u H_0 & \dots & B_u H_{n_p-k} \end{bmatrix}, & k \in \mathbb{I}_{[1,n_p]} \end{cases}$$

Here $H_i := -(r + B_u^T V B_u)^{-1} B_u^T \Phi^i V B_w$; V and Φ are defined in Lemma 1.

The predicted control sequence from the auxiliary prediction system (23) is

$$\bar{u}(k) = K_x A_K^i x + (\boldsymbol{B}_{1,k} + \boldsymbol{B}_{2,k})\tilde{\boldsymbol{w}} + \boldsymbol{N}_k \boldsymbol{v}_{[0,n_p-1]} \tag{28b}$$

where $\boldsymbol{N}_k \in \mathbb{R}^{1 \times n_p}$ is

$$\boldsymbol{N}_k := \begin{bmatrix} K_x A_K^{k-1} B_u & K_x A_K^{i-2} B_u & \dots & K_x B_u & 1 & 0 & \dots & 0 \end{bmatrix}$$

and $\boldsymbol{B}_{1,k} \in \mathbb{R}^{1 \times n_p}$ is

$$\boldsymbol{B}_{1,k} := \begin{cases} 0_{n_x \times n_p}, & k = 0 \\ \begin{bmatrix} 0 & \dots & 0 & K_x B_u H_0 \dots & K_x B_u H_{n_p-k} \end{bmatrix}, & k \in \mathbb{I}_{[1,n_p-1]} \end{cases}$$

and $\boldsymbol{B}_{2,k} \in \mathbb{R}^{1 \times n_p}$ is

$$\boldsymbol{B}_{2,k} := \begin{bmatrix} 0 & \dots & 0 & B_u H_0 \dots & B_u H_{n_p-k} \end{bmatrix}$$

Remark 5. *Since the state constraint $\mathbb{X}$, input constraint $\mathbb{U}$, disturbance bound $\mathbb{W}$ and the MOAS Σ defined in* (22) *are all polytopes, the tightened state constraints $\mathbb{X}_k$, tightened control input constraints $\mathbb{U}_k$ and terminal constraints $\mathbb{X}_T$ are all polytopes and can be expressed by*

$$\begin{aligned} \mathbb{X}_k &= \{x \in \mathbb{R}^{n_x} : \boldsymbol{f}_{x,k} x \le \boldsymbol{g}_{x,k}\} \\ \mathbb{U}_k &= \{u \in \mathbb{R} : \boldsymbol{f}_{u,k} u \le \boldsymbol{g}_{u,k}\} \\ \mathbb{X}_T &= \{x \in \mathbb{R}^{n_x} : \boldsymbol{f}_{x,T} x \le \boldsymbol{g}_{x,T}\} \end{aligned} \tag{29}$$

where $\boldsymbol{f}$ and $\boldsymbol{g}$ are the support vectors of the corresponding polytopes.

The state and input constraints can be expressed by

$$\begin{aligned}\Gamma_x \boldsymbol{v}_{[0,n_p-1]} + \Lambda_x x + \Pi_x \tilde{\boldsymbol{w}} \le \eta_x \\ \Gamma_u \boldsymbol{v}_{[0,n_p-1]} + \Lambda_u x + \Pi_u \tilde{\boldsymbol{w}} \le \eta_u\end{aligned} \tag{30a}$$

where Γ_x, Γ_u, Λ_x, Λ_u, Π_x, Π_u, η_x and η_u are defined by

$$\Gamma_x = \begin{bmatrix} \boldsymbol{f}_{x,0}\boldsymbol{M}_0 \\ \boldsymbol{f}_{x,1}\boldsymbol{M}_1 \\ \vdots \\ \boldsymbol{f}_{x,n_p-1}\boldsymbol{M}_{n_p-1} \end{bmatrix} \quad \Lambda_x = \begin{bmatrix} \boldsymbol{f}_{x,0} \\ \boldsymbol{f}_{x,1}A_K \\ \vdots \\ \boldsymbol{f}_{x,n_p-1}A_K^{n_p-1} \end{bmatrix}$$

$$\Gamma_u = \begin{bmatrix} \boldsymbol{f}_{u,0}\boldsymbol{N}_0 \\ \boldsymbol{f}_{u,1}\boldsymbol{N}_1 \\ \vdots \\ \boldsymbol{f}_{u,n_p-1}\boldsymbol{N}_{n_p-1} \end{bmatrix} \quad \Lambda_x = \begin{bmatrix} \boldsymbol{f}_{u,0}K_x \\ \boldsymbol{f}_{u,1}K_xA_K \\ \vdots \\ \boldsymbol{f}_{u,n_p-1}K_xA_K^{n_p-1} \end{bmatrix}$$

$$\Pi_x = \begin{bmatrix} \boldsymbol{f}_{x,0}\boldsymbol{C}_0 \\ \boldsymbol{f}_{x,1}\boldsymbol{C}_1 \\ \vdots \\ \boldsymbol{f}_{x,n_p-1}\boldsymbol{C}_{n_p-1} \end{bmatrix} \quad \Pi_u = \begin{bmatrix} \boldsymbol{f}_{x,0}(\boldsymbol{B}_{1,0}+\boldsymbol{B}_{2,0}) \\ \boldsymbol{f}_{x,1}(\boldsymbol{B}_{1,1}+\boldsymbol{B}_{2,1} \\ \vdots \\ \boldsymbol{f}_{x,n_p-1}(\boldsymbol{B}_{1,n_p-1}+\boldsymbol{B}_{2,n_p-1}) \end{bmatrix}$$

$$\eta_x = \begin{bmatrix} \boldsymbol{g}_{x,0} \\ \boldsymbol{g}_{x,1} \\ \vdots \\ \boldsymbol{g}_{x,n_p-1} \end{bmatrix} \quad \eta_u = \begin{bmatrix} \boldsymbol{g}_{x,0} \\ \boldsymbol{g}_{u,1} \\ \vdots \\ \boldsymbol{g}_{u,n_p-1} \end{bmatrix}$$

and the terminal constraint satisfies

$$\boldsymbol{f}_{x,T}\boldsymbol{M}_{n_p}\boldsymbol{v}_{[0,n_p-1]} + \boldsymbol{f}_{x,T}A_K^{n_p}x + \boldsymbol{f}_{x,T}\boldsymbol{C}_{n_p}\tilde{\boldsymbol{w}} \le \boldsymbol{g}_{x,T} \tag{30b}$$

where $\boldsymbol{M}$, $\boldsymbol{N}$, $\boldsymbol{C}$ and $\boldsymbol{B}$ are defined in (28), and $\mathbf{f}$ and $\mathbf{g}$ are defined in (29). Then the resulting QP problem is

$$\boldsymbol{v}^*_{[0,n_p-1]} = \arg\min_{\boldsymbol{v}_{[0,n_p-1]}} (27) \text{ s.t. } (30) \tag{31}$$

4.2. Implementations of the feedback noncausal MPC

In previous sections, the feedback noncausal MPC control algorithm is designed based on the assumption that the full information of x is available. However, in many cases, the direct measurements of all states of a WEC are not realistic, e.g. the states associated with the radiation force and excitation force. Thus a state observer needs to be designed. Assume the measured states are

$$y(k) = Cx(k) \tag{32}$$

and (A, C) is assumed to be observable. In this paper, a Luenberger observer is designed with the form of

$$\tilde{x}(k+1) = A\tilde{x}(k) + B_u u(k) + B_w\tilde{w}(k) + L(y(k) - C\tilde{x}(k)) \tag{33}$$

where $\tilde{x}$ is the estimated states and $\tilde{w}$ is the measured current wave elevation. In practical implementation, the observer gain L needs to be designed appropriately to achieve a satisfactory convergence of state estimation error within the computational limitation of the microprocessor.

The implementation of the proposed WEC feedback noncausal MPC framework is shown in Fig. 4. At each time step, with the wave prediction $\tilde{\boldsymbol{w}}$ provided by the wave prediction technology and the state estimation $\tilde{x}$ provided by the estimator (33), an online optimisation is solved and the corresponding feedback noncausal MPC control input is derived via Algorithm 2.

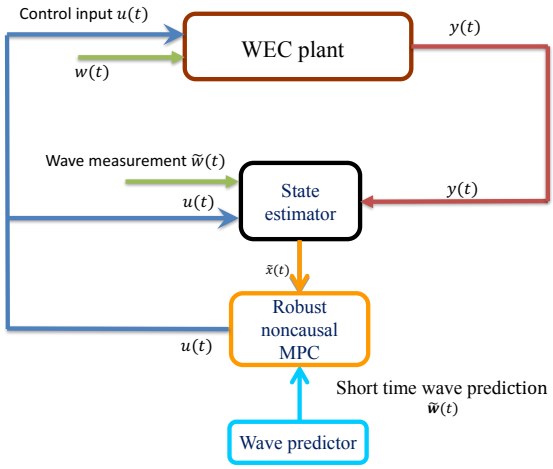

Figure 4: WEC feedback noncausal MPC framework

Algorithm 2. *The feedback noncausal MPC can be implemented by recursively going through the following procedure at each time step*

1. *Wave prediction $\tilde{\boldsymbol{w}}$ from wave prediction device.*
2. *State estimation updates:*

$$\tilde{x}(k) = \tilde{x}(k|k-1) + L(y(k) - C\tilde{x}(k|k-1)) \tag{34}$$

where $\tilde{x}(k|k-1)$ represents $\tilde{x}(k)$ estimated at time $k-1$, and L is designed offline.

3. *Control input update:*

$$u(k) = K_x\tilde{x}(k) + K_d\tilde{\boldsymbol{w}}(k) + v_0^* \tag{35}$$

where K_x and K_d are the linear noncasual optimal control gains defined offline from Lemma 1; v_0^* is the first element of the solution of the optimisation (31).

4. *Estimator updates:*

$$\tilde{x}(k+1|k) = A\tilde{x}(k) + B_u u(k) + B_w\tilde{w}(k) \tag{36}$$

where $\tilde{w}$ is the measured current wave elevation.

5. Numerical simulations

This Section presents three sets of simulation results to show the efficacy of the proposed feedback noncausal MPC method, and validates its robustness against wave prediction error. In Subsection 5.1, a set of simulations based on a reduced-order model will be provided for geometric visualisation of the satisfaction of recursive feasibility. To show the efficacy of the feedback noncausal MPC, another set of the simulations are presented based on a high-order model in Subsection 5.2. Finally, the influence of wave prediction error on the control response is demonstrated by simulations.

5.1. *Simulation set 1: Constraint handling using the constraint tightening approach*

The simulation in Subsection 5.1 is based on a reduced-order model, which is derived using a static excitation coefficient D_e and a static radiation coefficient D_r to approximate the dynamical realisations of (8) and (9). This results in a 2^{nd}-order state-space model

$$A_c = \begin{bmatrix} 0 & 1 \\ -\frac{k_s}{m} & -\frac{D_r}{m} \end{bmatrix} \quad B_{wc} = \begin{bmatrix} 0 \\ \frac{D_e}{m} \end{bmatrix} \quad B_{uc} = \begin{bmatrix} 0 \\ \frac{1}{m} \end{bmatrix}$$
$$C_z = \begin{bmatrix} 0 & 1 \end{bmatrix} \tag{37}$$

where $w := z_w$, $z := \dot{z}_v$, $x := [z_v, \dot{z}_v]$. The parameters are summarised in Table 1

Table 1: The parameters used for the 2^{nd}-order model in simulation set 1

Description	Notation	values
Stiffness	k_s	6.39×10^5 N/m
Float mass	m_s	7×10^3 kg
Added mass	m_a	1×10^3 kg
Total mass	m	8×10^3 kg
Input force limit	$u_{\max}$	2×10^5 N
Heave displacement limit	$d_{\max}$	1 m
Heave velocity limit	$v_{\max}$	3 m/s
Radiation coefficient	D_r	2×10^5 kg/s
Excitation coefficient	D_e	4×10^3 kg/s^2

After discretising the system with a sampling time $t_s = 0.1$ s, the feedback noncausal MPC is formulated using Algorithm 2. A $t_p = 0.5$ s or equivalently $n_p = 5$ of wave prediction is assumed to be available from a wave prediction technique. The objective function adopted is described in (16), where Q and r are tuned to be small enough to maximise energy output while the DARE (17d) still yields a unique stabilising solution. The controller gains K_x and K_d are computed using (17). The observer gain L is appropriately tuned to be sufficiently large to guarantee the accurate state estimation $\tilde{x} \approx x$.

The existence of a feedback noncausal MPC that guarantees recursive feasibility is determined by the existence of the MOAS (22). In this case, the largest wave magnitude that the WEC can operate safely is 1.15 m.

Fig. 5 shows the MOAS of the system (12) with terminal local controller K_x (22) and state and input constraints $|x_1| \leq 1$ m, $|x_2| \leq 3$ m/s and $|u| \leq 20$ kN respectively subject to assumed maximal disturbance $|w| \leq 1$ m. Fig. 6 and Fig. 7 show the tightened state and input constraints (24) for auxiliary prediction system (23) respectively. The size of tightened constraints shrinks with the increase of prediction steps k. Figs. 5-7 are computed using YALMIP (Löfberg, 2004) and Multi-Parametric Toolbox (MPC) (Herceg et al., 2013).

Next, time simulations are presented with a segment of real wave heave elevations for a period of 200 s gathered off the coast of Cornwall, UK. Fig. 8 indicates that whilst the wave elevations are bounded by the assumed maximal wave magnitude $|w| \leq 1$ m for most of the time, there are a few exceptions,

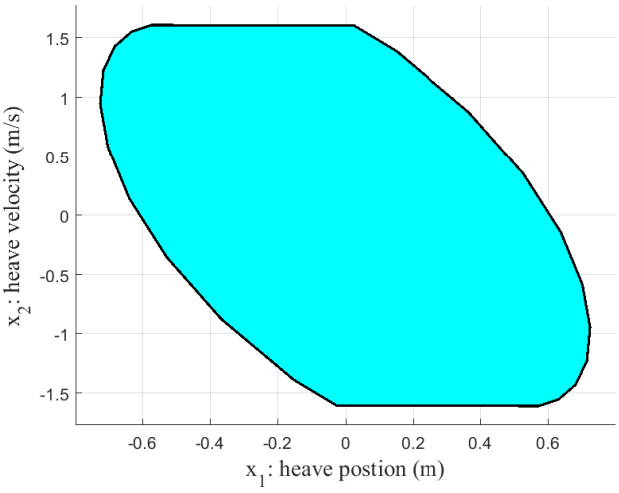

Figure 5: MOAS Σ with state constraints $|x_1| \leq 1$ m, $|x_2| \leq 3$ m/s and input constraints $u \leq 20$ kN subject to disturbance $|w| \leq 1$ m.

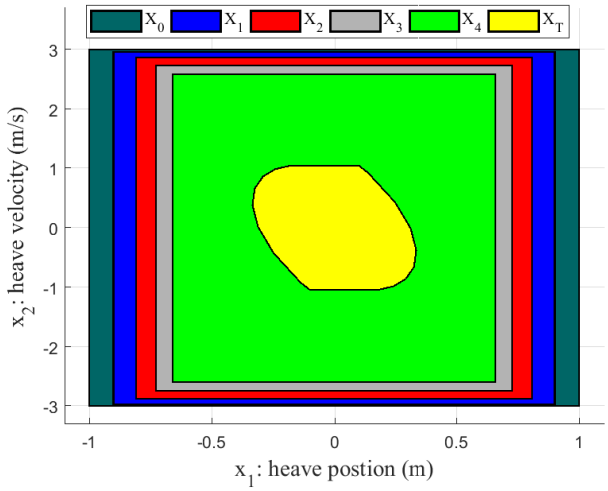

Figure 6: Tightened state constraints $\mathbb{X}_k$ and tightened terminal constraints $\mathbb{X}_T$ for auxiliary prediction system (23)

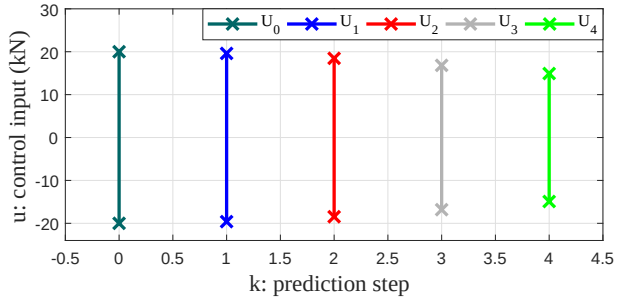

Figure 7: Tightened input constraints $\mathbb{U}_k$ for auxiliary prediction system (23)

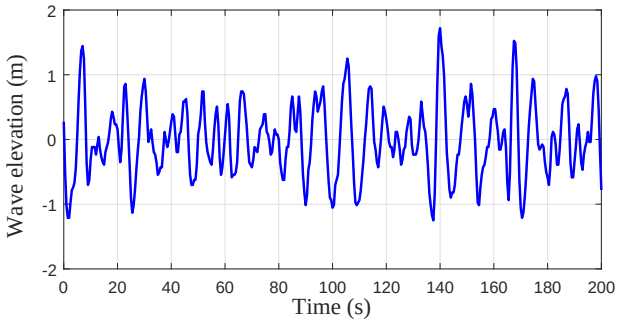

Figure 8: A 200 s period of real sea wave profile is used in simulations

especially at 7 s 140 s and 168 s. This wave profile is used in the following simulations to further show the efficacy of our proposed feedback noncausal MPC method in coping with constraints.

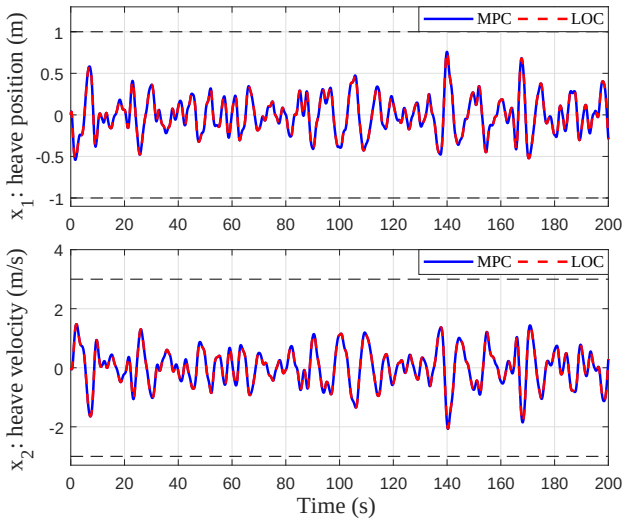

Figure 9: State trajectories

In Figs 9-10, comparative simulation results are presented using the feedback noncausal MPC based on Algorithm 2 and the corresponding linear noncausal optimal control with the same coefficients K_x and K_d. Fig. 9 and Fig. 10 show the state and input responses respectively. Whilst the state constraints are strictly satisfied and inactive for all the time using both controllers, the input constraint violations occur at $t = 7$ s, $t = 140$ s and $t = 168$ s using the linear noncausal optimal control (LOC), which roughly match the time instances when the wave peaks are significantly larger than 1 m in Fig. 8. However, the input constraint violations which occur when using the linear noncausal optimal control are avoided when the feedback noncausal MPC is adopted. When constraints are active at $t = 7$ s, $t = 140$ s and $t = 168$ s, it is shown in Fig. 10 that the auxiliary variable v comes into effect and keeps the input constraints satisfied. This clearly illustrates the advantage of the feedback noncausal MPC in explicitly handling constraints.

To show the energy conversion efficiency of the proposed feedback noncausal MPC subject to constraints, the perfor-

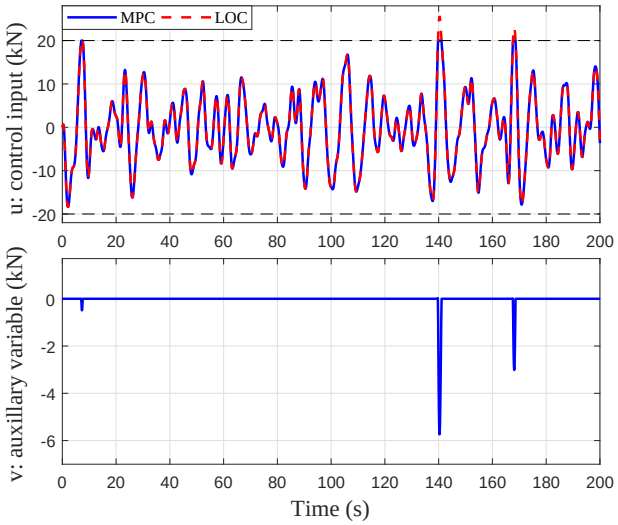

Figure 10: Input trajectories

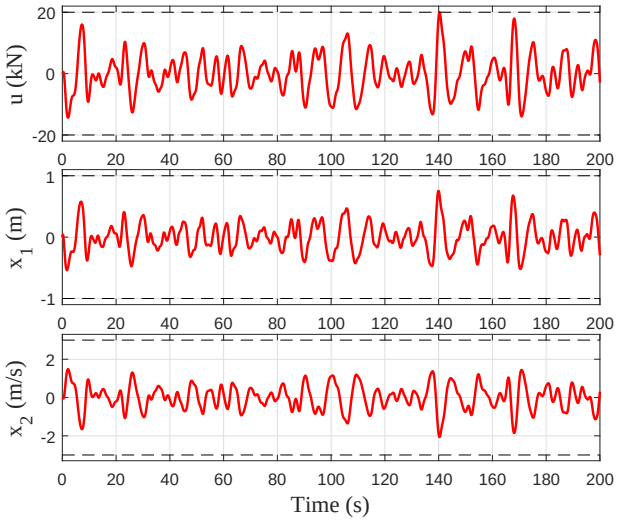

Figure 11: Input constraint and state constraints are strictly satisfied using retuned LOC

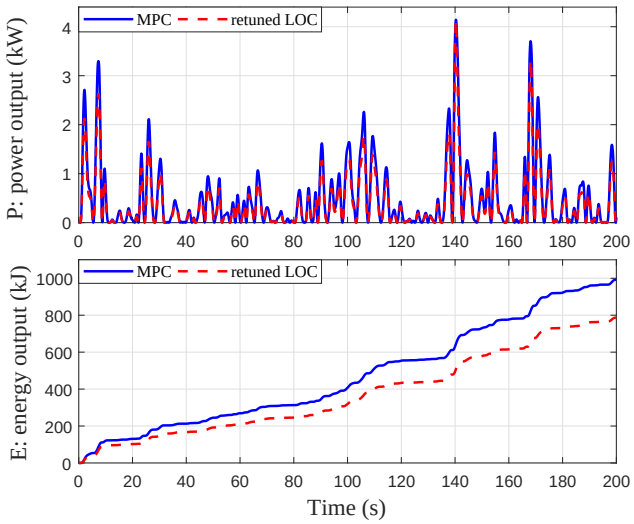

Figure 12: Energy output (992 KJ energy output when using the feedback noncausal MPC vs 787 KJ when using the retuned linear noncausal optimal control)

mance of the WEC using the feedback noncausal MPC is compared with that using the linear noncausal optimal control (Zhan and Li, 2018), whose weights are retuned to ensure the input constraint and state constraints are inactive during the simulation, as shown in Fig. 11. Fig. 12 compares the energy output when using these two controllers: 992 kJ of wave energy is converted when using the feedback noncausal MPC compared with 787 kJ when using the linear noncausal optimal control, which represents an increase of 26% increase of conversion efficiency.

The simulation results in Subsection 5.1 validate the efficacy of the feedback noncausal MPC to handle input and state constraints and also produce a good amount of wave energy output. Note that the computational burden using the proposed feedback MPC that requires online optimisation is obviously greater than the LOC, whose coefficients are all computed offline, with the time to perform 200 s of simulation being 14.76 s with MPC and 0.016 s with LOC, respectively. The proposed noncausal feedback MPC can still be implemented on economically viable microprocessor since the online optimisation problem is a convex QP, which can be efficiently resolved using mature optimisation method, e.g. interior point method or active set method.

5.2. *Simulation set 2: Demonstration of effectiveness of incorporating future wave predictions in MPC.*

In Subsection 5.2, the simulations are presented based on a full-order WEC model (11) to show the universal efficacy of our proposed feedback noncausal MPC. The parameters of this WEC are adopted from (Yu and Falnes, 1995) and summerised in Table 2.

The dynamic modelling of the radiation force (8) and excitation force (9) are given respectively by

$$A_r = \begin{bmatrix} 0 & 0 & -17.9 \\ 1 & 0 & -17.7 \\ 0 & 1 & -4.41 \end{bmatrix}, \quad B_r = \begin{bmatrix} 36.5 \\ 394 \\ 75.1 \end{bmatrix} \qquad (38)$$
$$C_r = \begin{bmatrix} 0 & 0 & 1 \end{bmatrix}$$

Table 2: The parameters used for the full-order model in simulation set 2

Description	Notation	values
Stiffness	k_s	3866 N/m
Float mass	m_s	242 kg
Added mass	m_a	83.5kg
Total mass	m	325.5 kg
Input force limit	$u_{\max}$	6 kN
Heave displacement limit	$d_{\max}$	0.5 m
Heave velocity limit	$v_{\max}$	1 m/s

and

$$A_e = \begin{bmatrix} 0 & 0 & 0 & 0 & -400 \\ 1 & 0 & 0 & 0 & -459 \\ 0 & 1 & 0 & 0 & -226 \\ 0 & 0 & 1 & 0 & -64 \\ 0 & 0 & 0 & 1 & -9.96 \end{bmatrix}, \quad B_e = \begin{bmatrix} 1549886 \\ -116380 \\ 24748 \\ -644 \\ 19.3 \end{bmatrix} \qquad (39)$$
$$C_e = \begin{bmatrix} 0 & 0 & 0 & 0 & 1 \end{bmatrix}$$

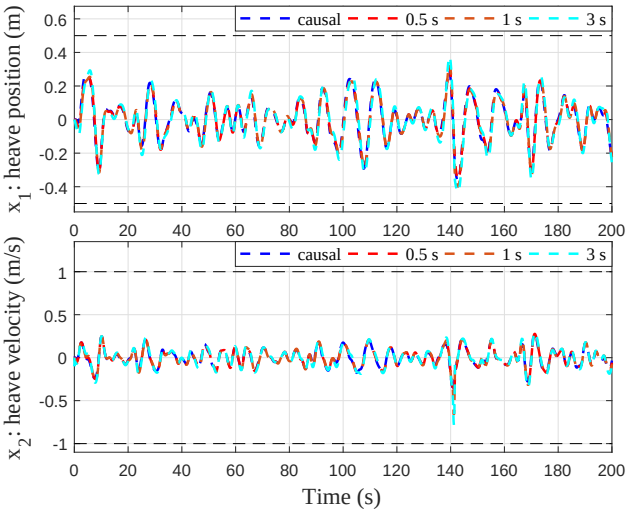

Figure 13: State trajectories

Three cases of the proposed feedback noncausal MPC with wave prediction length (t_p = 0.5 s, t_p = 1 s and t_p = 3 s) and a case with robust causal MPC proposed in (Zhan et al.) are compared to demonstrate the effectiveness of incorporating short time wave predictions in MPC design. The wave profile is irregular and appropriately scaled according to the size of the WEC.

Fig. 13 and Fig. 14 show the state and input trajectories for these cases respectively. The state and input constraints are satisfied all the time. Whilst the magnitude of wave feedforward part becomes greater with the increase of wave prediction length, the magnitude of the maximal control input signal does not have significant changes, which provides a fair comparison basis. Fig. 15 shows the power and energy outputs for four cases. The energy outputs with causal MPC and feedback

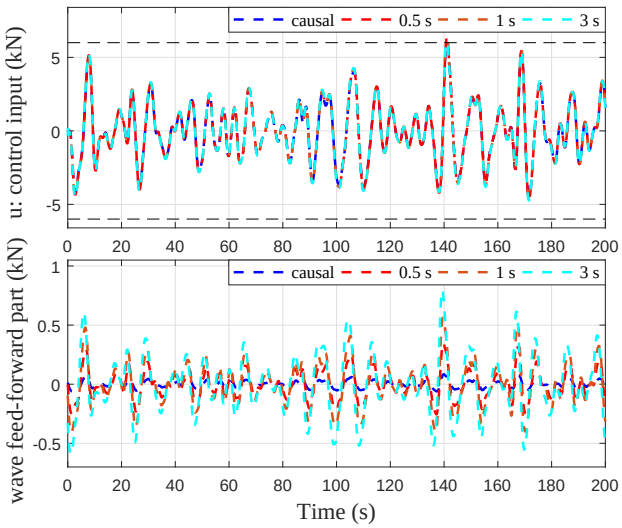

Figure 14: Input trajectories

noncausal MPC with wave prediction length of 0.5 s, 1 s and 3 s are 33.92 kJ, 35.91 kJ, 38.82 kJ and 43.15 kJ respectively, which represents 5.9%, 14.4% and 27.2% energy increases by incorporating wave predictions into the WEC MPC with prediction length of 0.5 s, 1 s and 3 s, respectively.

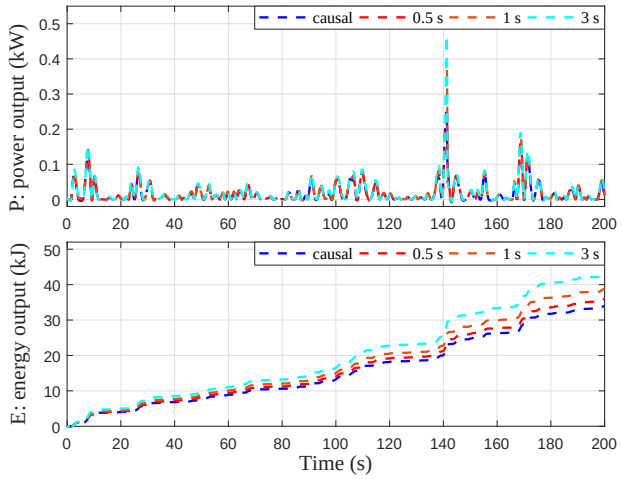

Figure 15: Energy output

5.3. *Simulation set 3: Influence of wave prediction error.*

In Subsection 5.2, the simulations are based on the 100% accurate wave prediction. However, prediction errors are inevitable for any wave prediction technique. To demonstrate the influence of the prediction errors on the proposed control strategy, a set of simulations are provided based on inaccurate wave prediction information. The WEC model and parameters used in this Subsection are the same with those used in the Subsection 5.2. The wave prediction length is 3 s.

To facilitate the simulation, at each time step, the wave prediction is assumed to have statistical wave prediction errors, where the discrepancies of the actual wave elevations and the predicted wave elevations increase with the length of the prediction time from the current time. Fig. 16 shows a snapshot of the predicted wave profiles with statistically added prediction errors from the current time step (shown in red dot lines) and the actual wave profile (shown in blue solid line). Note that for demonstration purpose, the wave prediction discrepancies used in the Simulation set 3 are intentionally chosen to be notably greater than those using the state-of-art wave forecasting techniques (Belmont et al., 2014; Fusco and Ringwood, 2010; Mérigaud and Ringwood, 2018).

Comparative simulations are obtained using

1. The feedback noncausal MPC with 3 s of perfect wave prediction information; the simulation results are referred as “Actual” shown in blue solid line;
2. The feedback noncausal MPC with 3 s of imperfect wave predictino information whose prediction error increases with the prediction time; the simulation results are referred as “Predicted” and shown in red dashed line.

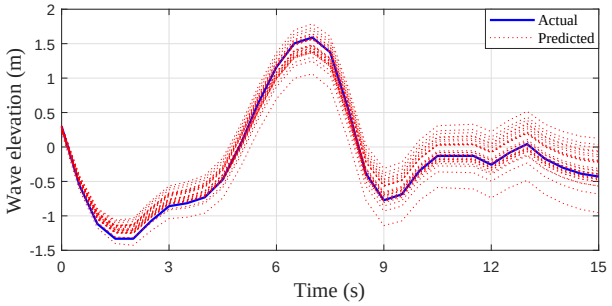

Figure 16: Inaccurate wave prediction with growing discrepancies using in Simulation set 3.

Fig. 17 shows the state and input responses for both cases. Compared with the feedback noncausal MPC based on accurate wave prediction, the state and input responses are very similar. Fig. 18 shows the comparative energy output. By using the inaccurate wave prediction, 42.50 kJ of energy is produced, which represents a 1.5% of performance degradation compared with the 43.15 kJ of energy conversion using the accurate wave prediction. This result shows that even when the wave prediction error is significant enough, the feedback noncausal MPC can still outperform the feedback causal MPC significantly, with a 25% of energy conversion increase, and thus the proposed noncausal feedback MPC is very robust to the wave prediction error.

6. Conclusion

This paper improves our previous result (Zhan et al.) by proposing a feedback noncausal MPC strategy for WECs that can directly incorporate short term wave prediction information into the WEC control to increase the energy output. This novel feedback noncausal MPC preserves the features of guaranteeing the recursive feasibility and robust constraint satisfaction. The sea condition for the WEC to safely operate can be explicitly calculated, which provides an important guideline for the

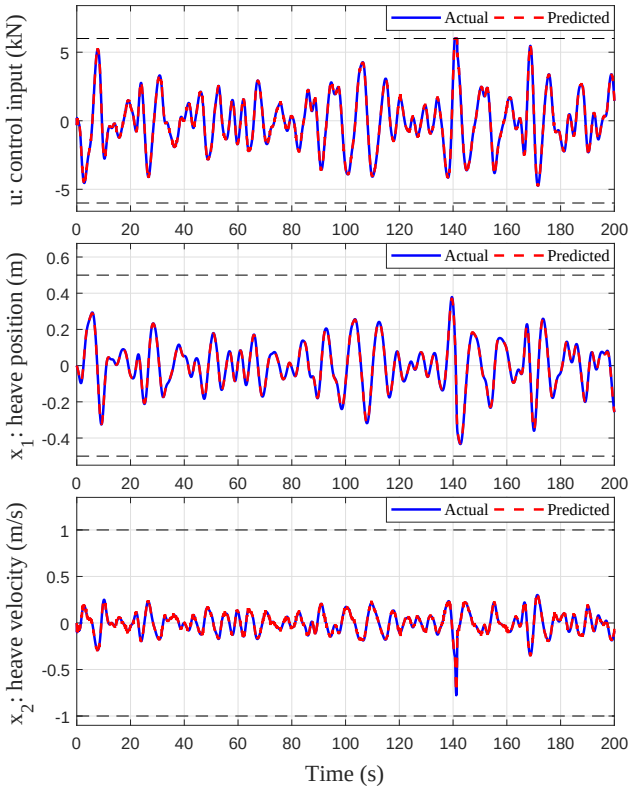

Figure 17: State and input trajectories using feedback noncausal MPC based on 3-s of wave prediction with/without prediction error.

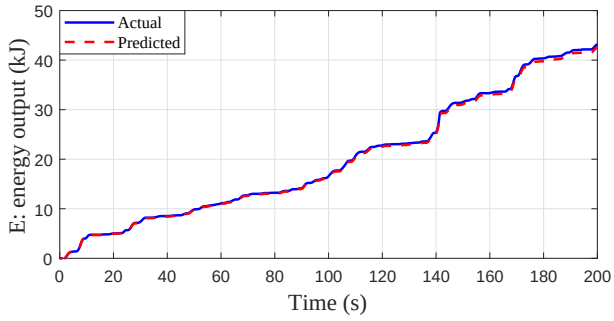

Figure 18: Energy output comparison between feedback noncausal MPCs based on accurate and inaccurate wave predictions.

WEC design and WEC controller tuning for guaranteeing safe operations. The proposed method can be potentially extended to a general class of energy conversion control problems. Since the associated mooring system in the PTO may affect the WEC dynamics though it can fit more realistic applications, we will further explore the applicability of the proposed control method for systems with mooring systems in our further work.

Acknowledgment

This work was supported by a Newton Mobility Grant, jointly funded by the Royal Society and NSFC (No. IE150833/ 6151101245) and National Natural Science Foundation of China (NSFC) (No. 61573174), the Newton Advanced Fellowship from The Royal Society, UK, under Grant NA160436, and in part a contract with Wave Energy Scotland on control system design of wave energy converters.

References

Amann, K.U., Magaña, M.E., Sawodny, O., 2015. Model predictive control of a nonlinear 2-body point absorber wave energy converter with estimated state feedback. IEEE Transactions on Sustainable Energy 6, 336–345.

António, F.d.O., 2008. Phase control through load control of oscillating-body wave energy converters with hydraulic pto system. Ocean Engineering 35, 358–366.

Babarit, A., Clément, A.H., 2006. Optimal latching control of a wave energy device in regular and irregular waves. Applied Ocean Research 28, 77–91.

Babarit, A., Guglielmi, M., Clément, A.H., 2009. Declutching control of a wave energy converter. Ocean Engineering 36, 1015–1024.

Baker, N., Mueller, M.A., 2001. Direct drive wave energy converters. Power Engineering 1, 1–7.

Belmont, M., Christmas, J., Dannenberg, J., Hilmer, T., Duncan, J., Duncan, J., Ferrier, B., 2014. An examination of the feasibility of linear deterministic sea wave prediction in multidirectional seas using wave profiling radar: Theory, simulation, and sea trials. Journal of Atmospheric and Oceanic Technology 31, 1601–1614.

Bemporad, A., Morari, M., 1999. Robust model predictive control: A survey. Robustness in Identification and Control , 207–226.

Brekken, T.K., 2011. On model predictive control for a point absorber wave energy converter, in: In Proceedings of the 2011 IEEE Trondheim on PowerTech, IEEE. pp. 1–8.

Budar, K., Falnes, J., 1975. A resonant point absorber of ocean-wave power. Nature 256, 478–479.

Chisci, L., Rossiter, J.A., Zappa, G., 2001. Systems with persistent disturbances: predictive control with restricted constraints. Automatica 37, 1019–1028.

Cretel, J.A., Lightbody, G., Thomas, G.P., Lewis, A.W., 2011. Maximisation of energy capture by a wave-energy point absorber using model predictive control. In Proceedings of the 18th IFAC World Congress 44, 3714–3721.

Drew, B., Plummer, A.R., Sahinkaya, M.N., 2009. A review of wave energy converter technology.

Faedo, N., Scarciotti, G., Astolfi, A., Ringwood, J.V., 2018. Energy-maximising control of wave energy converters using a moment-domain representation. Control Engineering Practice 81, 85–96.

Falnes, J., 2002. Ocean waves and oscillating systems: linear interactions including wave-energy extraction. Cambridge university press.

Falnes, J., 2007. A review of wave-energy extraction. Marine Structures 20, 185–201.

Fusco, F., Ringwood, J.V., 2010. Short-term wave forecasting for real-time control of wave energy converters. IEEE Transactions on Sustainable Energy 1, 99–106.

Fusco, F., Ringwood, J.V., 2013. A simple and effective real-time controller for wave energy converters. IEEE Transactions on Sustainable Energy 4, 21–30.

Goulart, P.J., Kerrigan, E.C., Maciejowski, J.M., 2006. Optimization over state feedback policies for robust control with constraints. Automatica 42, 523–533.

Hals, J., Falnes, J., Moan, T., 2011. Constrained optimal control of a heaving buoy wave-energy converter. Journal of Offshore Mechanics and Arctic Engineering 133, 011401.

Henderson, R., 2006. Design, simulation, and testing of a novel hydraulic power take-off system for the pelamis wave energy converter. Renewable Energy 31, 271–283.

Herceg, M., Kvasnica, M., Jones, C., Morari, M., 2013. Multi-Parametric Toolbox 3.0. In Proceedings of the European Control Conference, Zürich, Switzerland, 2013 , 502–510.

Kim, T.H., Takao, M., Setoguchi, T., Kaneko, K., Inoue, M., 2001. Performance comparison of turbines for wave power conversion. International Journal of Thermal Sciences 40, 681–689.

Kolmanovsky, I., Gilbert, E.G., 1995. Maximal output admissible sets for discrete-time systems with disturbance inputs. In proceedings of the American Control Conference 3.

Lee, C., 1995. Wamit user manual .

Lee, Y.I., Kouvaritakis, B., 2000. Robust receding horizon predictive control for systems with uncertain dynamics and input saturation. Automatica 36, 1497–1504.

Li, G., 2017. Nonlinear model predictive control of a wave energy converter based on differential flatness parameterisation. International Journal of Control 90, 68–77.

Li, G., Belmont, M.R., 2014. Model predictive control of sea wave energy converters–part i: A convex approach for the case of a single device. Renewable Energy 69, 453–463.

Li, G., Weiss, G., Mueller, M., Townley, S., Belmont, M.R., 2012. Wave energy converter control by wave prediction and dynamic programming. Renewable Energy 48, 392–403.

Lima, C., Gomes, V., Lima, J., Martins, J.F., Barata, J., Ribeiro, L., Cândido, G., 2011. A standard-based software infrastructure to support energy efficiency using renewable energy sources , 1175–1180.

Löfberg, J., 2004. Yalmip : A toolbox for modeling and optimization in matlab. In Proceedings of the CACSD Conference, Taipei, Taiwan, 2004 .

Mayne, D.Q., Rawlings, J.B., Rao, C.V., Scokaert, P.O., 2000. Constrained model predictive control: Stability and optimality. Automatica 36, 789–814.

Mérigaud, A., Ringwood, J.V., 2018. Incorporating ocean wave spectrum information in short-term free-surface elevation forecasting. IEEE Journal of Oceanic Engineering .

Mérigaud, A., Ringwood, J.V., 2018. Towards realistic non-linear receding-horizon spectral control of wave energy converters. Control Engineering Practice 81, 145–161.

Mueller, M., 2002. Electrical generators for direct drive wave energy converters. IEE Proceedings-Generation, Transmission and Distribution 149, 446–456.

Richter, M., Magana, M.E., Sawodny, O., Brekken, T.K., 2013a. Nonlinear model predictive control of a point absorber wave energy converter. IEEE Transactions on Sustainable Energy 4, 118–126.

Richter, M., Magaña, M.E., Sawodny, O., Brekken, T.K., 2013b. Power optimisation of a point absorber wave energy converter by means of linear model predictive control. IET Renewable Power Generation 8, 203–215.

Salter, S.H., 1974. Wave power. Nature 249, 720–724.

Salter, S.H., Taylor, J., Caldwell, N., 2002. Power conversion mechanisms for wave energy. Journal of Engineering for the Maritime Environment 216, 1–27.

Thorpe, T.W., et al., 1999. A brief review of wave energy. Harwell Laboratory, Energy Technology Support Unit.

Yu, Z., Falnes, J., 1995. State-space modelling of a vertical cylinder in heave. Applied Ocean Research 17, 265–275.

Zhan, S., He, W., Li, G., . Robust feedback model predictive control of sea wave energy converters. In Proceedings of the 20th IFAC World Congress, Toulouse, France, 2017 .

Zhan, S., Li, G., 2018. Linear noncausal optimal control of wave energy converters. IEEE Transactions on Control System Technology .